[19]G. Nilsson and S. Rolandson (unpublished).
[20]G. Gilat and L. J. Raubenheimer, Phys. Rev. 144, 390 (1966).
[21]D. L. Martin, Can. J. Phys. 38, 17 (1960).
[22]T. C. Cetas, C. R. Tilford, and C. A. Swenson, Phys. Rev. 174, 835 (1968).
[23]L. Van Hove, Phys. Rev. 89, 1189 (1953).
[24]W. Bührer, Eidgenoessisches Inst. fuer Reaktorforschung Report No. 174, Würenlingen, Switzerland, 1970 (unpublished).
[25]A. P. Miller and B. N. Brockhouse, Can. J. Phys. 49, 704 (1971).

PHYSICAL REVIEW B VOLUME 7, NUMBER 6 15 MARCH 1973

Giant Quantum Oscillations in the Magnetoacoustic Attenuation of Mercury*

G. Bellessa
Laboratoire de Physique des Solides,† Bâtiment 510, Faculté des Sciences, 91-Orsay, France
(Received 2 August 1972)

Measurements of the magnetoacoustic attenuation have been performed in mercury single crystals at temperatures down to 0.45 K and fields up to 70 kOe. For longitudinal waves in the frequency range 20–70 MHz, the attenuation coefficient exhibits giant quantum oscillations with spikelike character. The attenuation peaks are induced by the β arms of the first-zone hole surface. Their period in inverse magnetic field is measured as a function of the magnetic field orientation. The particular shape of the attenuation peaks is explained by taking into account the negative value of the effective mass in the magnetic field direction (saddle point). Measurements of the linewidth and height are presented. It is shown that the line suffers an inhomogeneous broadening. The latter is connected with the effect of dislocations on the Landau levels and a line-shape calculation is presented. Unusual line-height properties are reported. The line height depends on the ultrasonic-wave amplitude and in some cases there are attenuation dips instead of attenuation peaks at the same magnetic field values. The peak-height behavior is explained by a magnetic field effect on the electron-dislocation interaction.

I. INTRODUCTION

The giant quantum oscillations (GQO) in the magnetoacoustic attenuation in metals have been predicted by Gurevitch *et al.*[1] According to the theory, the GQO are peaks in the acoustic attenuation versus magnetic field. The latter arise from the resonant absorption of the sound wave by the electrons which move along the magnetic field with the sound velocity (in the simplest case where the wave vector is parallel to the magnetic field). The GQO have been observed in zinc,[2,3] rhenium,[4] bismuth,[5–8] gallium,[9] arsenic,[10] and mercury,[11] but it is only in the four last materials that the GQO exhibit a spikelike character. By studying the shape of the attenuation peaks, one can obtain information about the cyclotron mass, the g factor, and the relaxation time. It is the purpose of this paper to report the results of such a study in mercury.

The main parts of the paper are Sec. II, a brief description of the GQO theory and new theoretical calculations about the line shape; Sec. III, a description of the experimental procedure; Sec. IV, the presentation of the experimental results; and Sec. V, the interpretation of some GQO-peak properties with a magnetic field effect on the electron-dislocation interaction.

II. THEORY

The GQO theory has been established by Gurewitch *et al.*[1] for the free-electron case. In the case of mercury, we shall deal with quasicylindrical Fermi surfaces. Therefore, we refer in this part to the theory of Kaner and Skobov,[12] who have taken a nonisotropic energy-momentum law for the electrons. One can write for the electron energy in the presence of an uniform magnetic field $\vec{H}$ along the z axis

$$E_n(k_z) = n\hbar\Omega + \hbar^2 k_z^2/2m_{\parallel} , \tag{1}$$

where n is the Landau-level number, Ω is the cyclotron frequency $eH/m_c c$, and k_z is the z component of the electron wave vector. The effective mass $m_{\parallel}$ in the magnetic field direction is defined by the relation

$$\frac{1}{m_{\parallel}} = \frac{1}{\hbar}\left(\frac{\partial}{\partial k_z}\langle v_z\rangle_{\mathrm{av}}\right)_0 = \frac{1}{2\pi m_c}\left(\frac{\partial^2 A}{\partial k_z^2}\right)_0 , \tag{2}$$

where $A(k_z)$ is the area of the intersection of the Fermi surface with a plane perpendicular to $\vec{H}$. We omit index k_y in Eq. (1) because the energy does not depend on this quantum number. Nevertheless, we take it into account when we replace the sum over states by an integral. For simplicity, we have written neither the spin term nor the phase term

in Eq. (1). The latter is $\frac{1}{2}\hbar\Omega$ in the free-electron case.

For large values of the electron mean free path, a sound wave of frequency ω and wave vector $\vec{q}$ which propagates in the metal can be regarded as a phonon beam and the acoustic-wave attenuation can be treated as the direct absorption of phonons by the electrons. Assuming conservation of energy and momentum, one obtains for an electron $E_n(k_z)$ which absorbs a phonon $(\omega, \vec{q})$ the condition

$$\hbar\Omega(n'-n) \simeq \hbar\omega - \hbar^2 q_z k_z / m_{\parallel}\,, \tag{3}$$

where q_z is the z component of $\vec{q}$. Experimentally, the magnetic field is high enough for the inequalities $\Omega \gg \omega$ and $\Omega \gg \hbar q_z k_z / m_{\parallel}$ to be satisfied. Hence, there is no Landau-level change as a result of the phonon absorption and condition (3) can be written in the form

$$k_z = k_0 \equiv m_{\parallel} V_s / \hbar \cos\theta\,, \tag{4}$$

where V_s is the sound velocity and θ the angle between $\vec{q}$ and $\vec{H}$. Condition (4) means that the only electrons which can absorb phonons are those drifting in phase with the acoustic wave. The concerned electrons evidently have to be on the Fermi surface to absorb phonons. Thus at zero temperature, when one sweeps the magnetic field, there is a peak in the sound absorption corresponding to each Landau level n. The magnetic field location of this peak is given by the relation $E_n(k_0) = E_F$, where E_F is the Fermi energy. The period of the attenuation peaks may be derived through a way similar to that used for the de Haas–van Alphen period calculation. One obtains for the period in inverse magnetic field

$$\Delta(1/H) = 2\pi e/\hbar c S, \tag{5}$$

where S is the area of the intersection of the Fermi surface with the plane $k_z = k_0$. Actually k_0 is very small (if the sound propagation direction is not perpendicular to $\vec{H}$) and one can consider S as the extremal cross section of the Fermi surface. Hence, Eq. (5) becomes identical to the de Haas–van Alphen period expression.

Up to now, we have not considered the temperature and collision effect on the GQO. When the temperature is nonzero, there are electron transitions in a bandwidth kT about E_F. Consequently, the peaks are broadened but they always exist as long as $kT \ll \hbar\Omega$. The effect of the electron scattering on the GQO is to destroy the selection rule (4) and to replace it by the less stringent condition[13]

$$k_0(1 - 1/\omega\tau) \le k_z \le k_0(1 + 1/\omega\tau), \tag{6}$$

where τ is the relaxation time of the electrons. From this relation, it appears that the selection rule loses its physical meaning when $\omega\tau < 1$. In this case, the GQO are no longer resulting from a resonant effect but rather from a variation of the density of states at the Fermi level. However, they can keep a spikelike character if the electron mean-free path satisfies the inequality[12]

$$q l_{\parallel} (\hbar\Omega/E_F)^{1/2} \gg 1, \tag{7}$$

where $l_{\parallel} = \tau(2E_F/m_{\parallel})^{1/2}$. Condition (7) means that the electrons which yield each sound absorption peak are located on a single Landau level.

The shape of the sound absorption peak gives information on the cyclotron mass and the electron scattering. Kaner and Skobov[12] have obtained a general expression for the sound absorption by the electrons:

$$\frac{Q}{Q_0} = \frac{\hbar^2\Omega q}{2\omega m_{\parallel}} \sum_n \int dE\, dk_z [f(E) - f(E+\hbar\omega)] \times D(E - E_n(k_z)) D(E + \hbar\omega - E_n(k_z + q)), \tag{8}$$

where Q_0 is the acoustical absorption when $H = 0$, $F(E)$ is the Fermi function, and $D(E)$ is a Lorentzian function

$$D(E) = \frac{1}{\pi} \frac{\hbar/2\tau}{E^2 + (\hbar/2\tau)^2}. \tag{9}$$

One can also derive Eq. (8) by treating the Landau-level broadening like Dingle[14] and by applying Fermi's Golden Rule. The effect of the electron-mass sign on the line shape has not been considered in the existing theories and we shall clarify this point starting from Eq. (8). In the case $kT \gg \hbar/\tau$ and $\omega\tau < 1$, which is the usual one, it is possible to integrate Eq. (8) over energy. For $m_{\parallel} > 0$, putting

$$y = \hbar k_z (2 m_{\parallel} k T)^{-1/2}, \tag{10}$$

one obtains[12]

$$\frac{Q}{Q_0} = \frac{\hbar\Omega}{2kT} \int_0^{\infty} dy\, \frac{1}{\pi} \frac{B}{1 + B^2 y^2} \times \sum_n \cosh^{-2}[\tfrac{1}{2}(y^2 - A_n)], \tag{11}$$

where

$$B = q l_{\parallel} (kT/E_F)^{1/2}, \quad A_n = (E_F - n\hbar\Omega)/kT. \tag{12}$$

Equation (11) is identical to the result of Gurevitch *et al.*,[1] provided that one replaces the electron mean free path $l = \tau V_F$ by $l_{\parallel}$ in Gurevitch's expression. If B is not too large with respect to 1 (i.e., if the collision broadening is not too small with respect to the thermal broadening), Eq. (11) gives an asymmetrical line shape[15]: The attenuation decreases faster than it increases when one increases the magnetic field. For $m_{\parallel} < 0$ (saddle point), it is no longer possible to write Eq. (10) in the same form. Substituting $|m_{\parallel}|$ for $m_{\parallel}$ in Eq. (10), we obtain for the electron energy

$$E_n(k_z) = n\hbar\Omega - y^2 kT. \tag{13}$$

The negative sign in Eq. (13) produces some modifications in the attenuation calculation. Having performed these corrections, one obtains[11]

$$\frac{Q}{Q_0}=\frac{\hbar\Omega}{2kT}\int_0^\infty dy\,\frac{1}{\pi}\frac{B}{1+B^2y^2}\sum_n \cosh^{-2}[\tfrac{1}{2}(y^2+A_n)]. \tag{14}$$

Equation (14) also gives an asymmetrical line shape, but now it is the low-field side which is sharper than the high-field side. Physically, this result means that the low-field side reflects the thermal broadening and the high-field side the collision broadening.

Now we are going to derive an expression for the attenuation peak which gives a temperature-independent linewidth in the case $kT \gg \hbar/\tau$. For a fixed value of B, Eqs. (11) and (14) give a linewidth which is proportional to the temperature. We shall see in Sec. IV that the linewidth can be temperature independent and this character will be connected with dislocations. Actually, the dislocations distort the crystal lattice and can induce an inhomogeneous broadening of the attenuation peak in the two following ways: (a) As a result of the smearing in Onsager's quantization rule,[16,17] and (b) due to the interaction of the electrons with the elastic field of the dislocation, there is an electron energy dependence in the real space $E(k,x)=E_0+C\Delta(x)+\hbar^2k^2/2m$.[18] In the two cases, instead of a single Landau level, we have now to consider a Landau-level distribution $G(U_n-U_n^0)$ which is centered about the energy $U_n^0=n\hbar\Omega$. Consequently, we obtain for the sound absorption by the electrons

$$\frac{Q}{Q_0}=\frac{\hbar^2\Omega q}{2\omega m_\parallel}\sum_n\int dU_n\,G(U_n-U_n^0)\times(KS), \tag{15}$$

where (KS) is the integral of Eq. (8) and $E_n(k_z)$ is defined by the relation

$$E_n(k_z)=U_n+\hbar^2k_z^2/2m_\parallel. \tag{16}$$

We consider the case $kT \ll X$, where X is the width of the Landau-level distribution. Then, we can replace the Fermi-function derivative by a Dirac function in Eq. (15). Upon integration we obtain

$$\frac{Q}{Q_0}=\hbar\Omega\int_0^\infty dy\,\frac{1}{\pi}\frac{B}{1+B^2y^2}\sum_n G((E_F-\tfrac{1}{2}y^2X)-U_n^0), \tag{17}$$

where

$$y=\hbar k_z(m_\parallel X)^{-1/2},\quad B=q\tau(X/m_\parallel)^{1/2}. \tag{18}$$

We take for the Landau-level distribution a Gaussian function

$$G(U_n-U_n^0)=(2/\pi X^2)^{1/2}\,e^{-4(U_n-U_n^0)^2/X^2}. \tag{19}$$

Then Eq. (17) becomes

$$\frac{Q}{Q_0}=\frac{\hbar\Omega}{\pi X}\left(\frac{2}{\pi}\right)^{1/2}\int_0^\infty dy\,\frac{B}{1+B^2y^2}\sum_n e^{-(A_n-y^2)^2}, \tag{20}$$

where

$$A_n=2(E_F-n\hbar\Omega)/X. \tag{21}$$

We have performed the calculation for $m_\parallel>0$. As in the homogeneous case, we should obtain for $m_\parallel<0$ a term $-(A_n+y^2)^2$ instead of $-(A_n-y^2)^2$ for the argument of the exponential function. When $B\gtrsim 1$, Eq. (20) gives a line shape similar to that given by Eq. (11) (Fig. 3), but now the linewidth is proportional to X and no more to kT.

III. EXPERIMENTAL PROCEDURE

The magnetoacoustic attenuation was measured by using the pulse-echo method at temperatures down to 0.4 K and in magnetic fields up to 70 kOe. rf pulses up to 70 MHz were generated by a pulsed oscillator and converted to ultrasound by a quartz transducer bonded to one of the two parallel sample surfaces. Quartz transducers were X cut (longitudinal waves) and isopentane was used as the bonding agent. The ultrasonic echoes were picked up by the same transducer, then amplified and demodulated. A box-car integrator selected one of the pulses and provided a voltage proportional to its amplitude. The magnetic field was produced by a superconducting magnet and the low temperatures were obtained with a He_3 cryostat.

Experiments were carried out on two mercury samples which were cut out of single crystals using a spark cutter at 77 K. The single crystals were grown by the Bridgman technique and their orientations were determined by the Laue x-ray technique at 77 K. The starting material was 99.9995%-pure mercury supplied by Jaeger company. Its residual resistivity ratio has been estimated at 5×10^5 elsewhere.[19] We shall refer to the two prepared crystals as samples 1 and 2. They had the following features:

Sample 1. It was a cylinder 5 mm thick with parallel and flat faces which were (100) planes. The crystal was put in a sample holder and could not be rotated. The magnetic field and the acoustic wave vector were parallel to the $[100]^*$ direction (see Ref. 20 for definition of $[100]^*$).

Sample 2. It was a cube having two faces perpendicular to the [100] direction and two others parallel to the $(01\bar{1})$ symmetry plane. The acoustic wave was propagated in the [100] direction. The crystal was mounted in a sample holder having two orthogonal axes of rotation. One horizontal axis was normal to the $(01\bar{1})$ plane of the crystal which could be rotated $\pm 90°$ round it. The second horizontal axis allowed the $(01\bar{1})$ plane to rotate $\pm 3°$. Thus it was possible to set accurately the magnetic field (which was vertical) in the $(01\bar{1})$ symmetry plane or to turn it out of this plane. A sample holder satisfying such conditions was required for the study of the GQO-peak splitting.

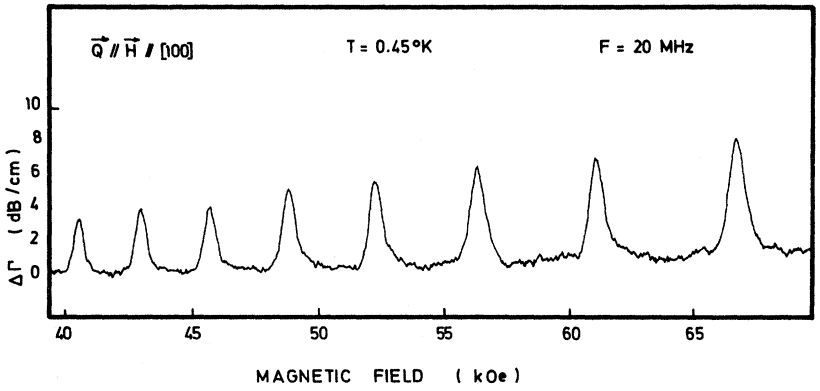

FIG. 1. Recorder tracing of the ultrasonic-attenuation change in mercury showing the GQO.

IV. RESULTS AND DISCUSSION

The GQO with spikelike character appear at magnetic fields above 20 kOe. Figure 1 shows a typical recorder tracing of the change in the acoustic attenuation as a function of magnetic field intensity. From the period measurement, we find that the attenuation peaks are caused by the β arms of the first-zone hole surface.[21,22]

A. Periods

In order to compare our results with those of the de Haas–van Alphen effect,[21,23] we use the notation $f(1/H) \equiv [\Delta(1/H)]^{-1}$. Table I shows that our values are in good agreement with those of Brandt and Rayne[21] and Poulsen *et al.*[23] We have plotted in Fig. 2 the variation of the GQO frequency $f(1/H)$ when the magnetic field is rotated in the $(01\bar{1})$ symmetry plane. When $\vec{H}$ is in the [111] direction there are two sets of peaks which are well separated. In this case the peak height corresponding to the β arms along [100] is three times larger than that corresponding to the β arms along [010] and [001]. This behavior may look surprising since the [111] direction is equivalent for all the β arms. However it is not the same with the [100] wave-vector direction and a deformation-potential anisotropy can explain this effect.

The spikelike character of the GQO allows us to determine accurately the magnetic field location of the peaks. Using Onsager's quantization rule, we can write the relation

$$(1/H_n) f = n + \phi, \tag{22}$$

where n is the number of the Landau level, H_n is the magnetic field location of the corresponding peak, and ϕ is the phase factor. Table II gives the experimental values of H_n and the corresponding $(n+\phi)$ obtained from Eq. (22). The experimental conditions were $T = 0.45$ K, $F = 20$ MHz, and $\vec{q} \parallel \vec{H} \parallel [100]$. Owing to the regular increase in the value of $(n+\phi)$, we can unambiguously determine the Landau-level numbers and deduce the phase

$$\phi = 0.94 \pm 0.05.$$

This experimental result is not in agreement with theory which predicts $\phi = \frac{1}{2}$.[17] Starting from the relation

$$E_F = (n+\phi)\,\hbar e\, H_n / m_c c, \tag{23}$$

then using Table II and $m_c = 0.16 m_0$,[21] we find for the Fermi energy (measured from the top of the

TABLE I. Frequencies of the GQO in comparison with the de Haas–van Alphen results.

Magnetic field direction	$10^{-5} f(1/H)$ (Oe) Present work	$10^{-5} f(1/H)$ (Oe) Brandt *et al.* (Ref. 21)	$10^{-5} f(1/H)$ (Oe) Poulsen *et al.* (Ref. 23)
[100]*	8.03 ± 0.04	8.15	7.99
[100]	7.29 ± 0.04	7.35	7.39
[111]	10.3 ± 0.05	10.6	10.4

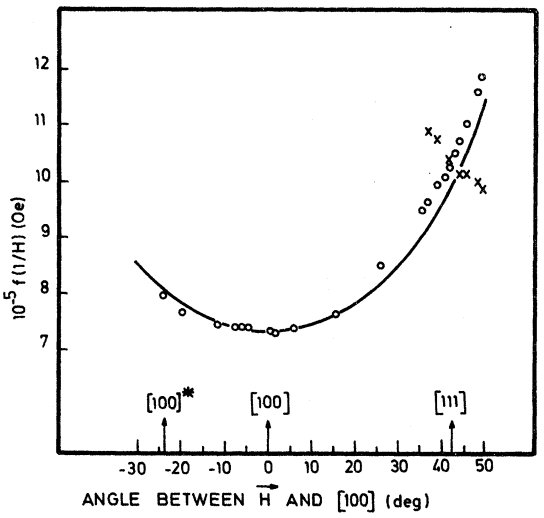

FIG. 2. GQO frequency as a function of magnetic field direction in the $(01\bar{1})$ symmetry plane. The circles are the experimental values of the β arms along [100]; the curve is the expected variation of cylinders along [100]. The crosses are the experimental values of the β arms along [010] and [001].

TABLE II. Determination of the Landau-level numbers when $\vec{q} \| \vec{H} \| [100]$, $T = 0.45$ K, and $F = 20$ MHz.

10^6 $(1/H)$ $(\mathrm{Oe})^{-1}$	$(1/H)\, f = n + \phi$
15.00	10.93
16.38	11.94
17.75	12.94
19.12	13.94
20.50	14.94
21.86	15.93
23.24	16.94
24.60	17.93
25.97	18.93
27.34	19.93
28.72	20.94
30.08	21.92
31.47	22.94
32.87	23.96
34.18	24.91
35.61	25.96
36.94	26.93
38.34	27.94
39.77	28.98
41.02	29.89
42.44	30.93

band)

$$E_F = 53 \times 10^{-3} \text{ eV}.$$

We have also derived ϕ and E_F in the experimental arrangement $\vec{q} \| \vec{H} \| [100]$*. The phase was found to be

$$\phi = 0.90 \pm 0.50,$$

while the Fermi energy remained the same as the previous one within 2%.

B. Line Shape

One can get information about cyclotron mass and electron mean free path from the line-shape analysis. Figure 3 shows a recorder tracing of an attenuation peak. The line is asymmetrical and the attenuation increases faster than it decreases when one increases the magnetic field. As we have seen in Sec. II, this shape can be explained by taking into account the negative sign of $m_{\|}$. Actually the β arms are more neck shaped than cylindrical (Fig. 2) and $m_{\|}$ is negative. Using Eq. (2) and the area variation of the β-arm cross section when the magnetic field is rotated (Fig. 2), the value of $m_{\|}$ can be estimated. It is found to be

$$m_{\|} \sim -m_0,$$

where m_0 is the free-electron mass. We have fitted the experimental line to the theoretical curve given by Eq. (14) (Fig. 3). Parameter B acts on the asymmetry of the curve[15,12] and is found to be 1.5 (i.e., $\tau \sim 10^{-9}$ sec). Integration in Eq. (14) was carried out with a computer and δA_n was found to be 4. It is easy to establish the relation between the theoretical width δA_n and the experimental one δH:

$$\frac{m_c}{m_0} = \frac{e\hbar f}{m_0 k T c H_0} \frac{\delta H}{\delta A_n}, \tag{24}$$

where H_0 is the magnetic field location of the peak. The result of the fit is

$$m_c = 0.36 m_0 .$$

This value is much larger than the value $m_c = 0.16 m_0$ which was determined by means of the de Haas–van Alphen effect[21] and the cyclotron resonance.[24] In order to explain this disagreement we have looked for a possible heating effect. In Eq. (24) we have used $T = 0.45$ K which was obtained from the temperature measurement of the helium bath but not that of the sample itself. Nevertheless, we were able to rule out any possibility of sample heating by acting on the pulse repetition rate of the generator. On the other hand, we can postulate neither a magnetic field inhomogeneity nor some crystal deformation to account for our linewidth. We were indeed able to observe the electron-lens quantum oscillations, the period of which was 100 Oe about 65 kOe. At last, our too-large linewidth may be caused by spin splitting. When the effective gyromagnetic factor $g^* = g m_c / m_0$ does not equal 2, each attenuation peak is split into two subpeaks which are more or less resolved. The m_c value of Brandt and Rayne[21] yields a linewidth $\delta H = 200$ Oe. In order to explain our 450-Oe-wide peak, the spin splitting has to be as large as 250 Oe, but then it has to resolve the two subpeaks. Thus, the spin-splitting

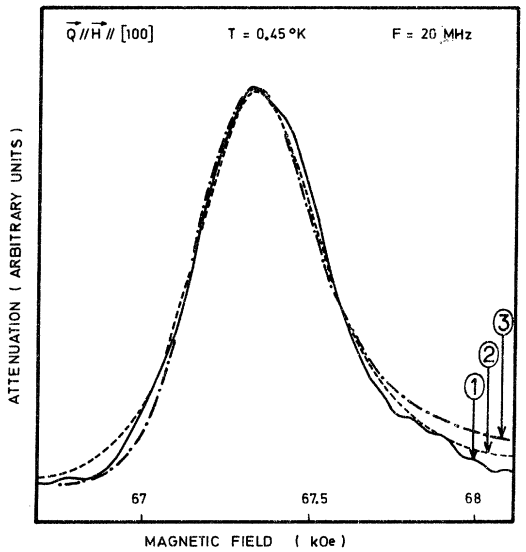

FIG. 3. Shape of an attenuation peak. 1, Experimental GQO peak; 2, curve obtained from Eq. (14); 3, curve obtained from Eq. (20).

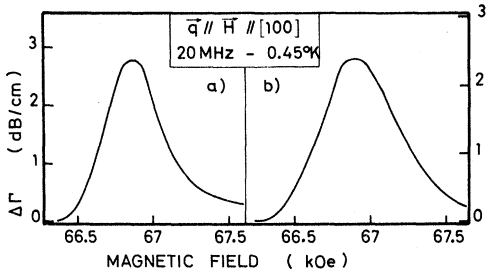

FIG. 4. Recorder tracing of a GQO peak showing the line broadening with the defect increase. (a) Peak of the first experiment; (b) peak after a thermal cycle and the production of a new sample-transducer bond.

hypothesis can be also ruled out.

Actually, the broadening of the attenuation peak is caused by defects as the following shows. In the first experiment on a crystal we have obtained 450 Oe for the peak width. Subsequent to the production of a new transducer-sample bond, which involved a rise of the temperature up to 130 K, the peak width was 640 Oe (Fig. 4). Thus, it is suggested that during the thermal cycle between 1 and 130 K and during the sample handling at 130 K, there has been a dislocation density increase leading to a line broadening. It may be seen in Fig. 4 that the attenuation peak is broadened without change of its shape. This behavior is not in agreement with a scattering effect, since the line asymmetry becomes in this case more pronounced when B is reduced. The broadening effect that we observe is indeed the first sign of the inhomogeneous character of the line. This will be confirmed in Sec. IV C.

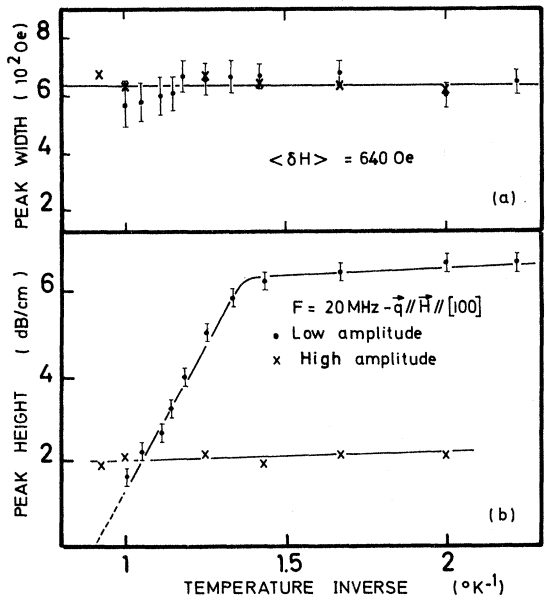

FIG. 5. Temperature dependence of the height and the width of the GQO peak located at 67 kOe. The high amplitude is 5 times larger than the low amplitude.

C. Temperature and Ultrasonic-Amplitude Effects

The experimental results depend on the temperature and the ultrasonic-wave amplitude. For a low amplitude[25] and for a given GQO peak (the one located at 67 kOe), we observe a temperature dependence of the height given by Fig. 5, the width being constant and equal to 640 Oe between 0.45 and 1.1 K. For a high ultrasonic amplitude, the peak width is the same as in the low-amplitude case but now there is no longer a temperature dependence of the peak height (Fig. 5).

In the low-amplitude case, the GQO peaks disappear about 1.1 K and attenuation dips appear. The latter are located at the same field values as the former. It has not been possible to measure the dip height in this temperature range, owing to the large magnetoacoustical noise. However the noise disappears at higher temperature and frequency and then the attenuation dips become very clear (Fig. 6). The dip height is also amplitude dependent.

The attenuation dips cannot be explained with the existing theories, and the GQO-peak behavior versus temperature and ultrasonic amplitude is not consistent with the GQO theory. The latter does not predict any ultrasonic-amplitude effect. Although it predicts a peak height inversely proportional to the temperature, it cannot explain the disappearance of the GQO peaks when the temperature increases, without the transformation of these peaks into the quantum oscillations of the de Haas-van Alphen type.[15] Lastly, theory predicts a linewidth proportional to the temperature in the case $kT \gg \hbar/\tau$. The preceding inequality was certainly realized in our experiments, since the geometrical resonances were always present at low field.[26] These oscillations disappear when $ql \lesssim 7$.[27] Thus we get $l \gtrsim 10^{-2}$ cm, i.e., $\tau > 10^{-10}$ sec. The line-

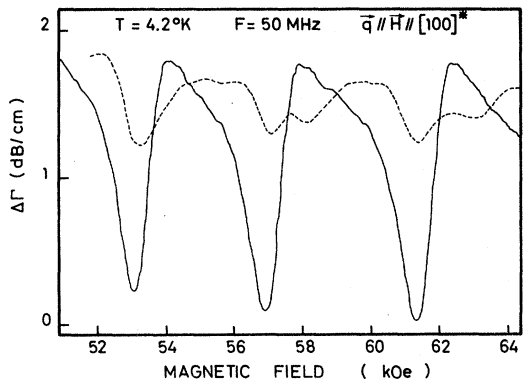

FIG. 6. Recorder tracing of the attenuation dips for a fixed ultrasonic amplitude. Dashed line, tracing from the first echo; solid line, that from the second echo.

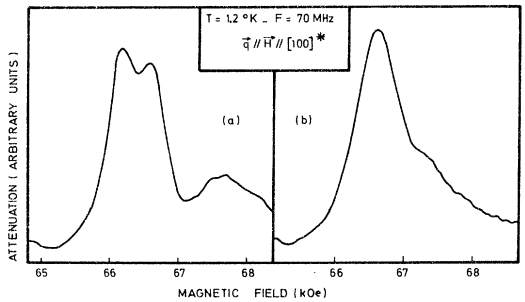

FIG. 7. Change in the recorder tracing of a GQO peak corresponding to a sample orientation change smaller than 0.3°.

width constancy can be explained with the inhomogeneous broadening that we have considered in Sec. II. We have fitted an experimental peak to the theoretical curve given by Eq. (20) (Fig. 3). As in the thermal-broadening case, B acts on the asymmetry of the curve and is found to be 1. Integration in Eq. (20) was carried out with a computer and δA_n was found to be 2.1. Using Eq. (21), we obtain for the dislocation broadening measured in Kelvin

$$X = 4.3 \text{ K}.$$

In the same way, we obtain $X = 6.5$ K for the sample which suffered a thermal cycle ($\delta H = 640$ Oe). Thus inequality $X \gg kT$ is satisfied and temperature has no effect on the linewidth.

D. Line-Shape Study at High Ultrasonic Frequency

The line shape has been studied at high ultrasonic frequencies (50–70 MHz) but the experimental conditions were not as good as at low frequency (20 MHz). When the ultrasonic frequency is increased the peak height is very large. Then it becomes difficult to record the top of the peak, especially as the apparatus sensitivity and the sample-transducer transmission decrease. Consequently it has not been possible to follow the line-shape evolution with temperature and acoustic-wave amplitude. The only study which has been done is at 1.1 K and with the highest pulse amplitude that the rf generator could deliver (about 400 V peak to peak). Using sample 1 at 1.2 K and 70 MHz (Fig. 7), we have observed a peak larger than those in the low-frequency case. The peak was split or not depending in a very critical way on the sample orientation with respect to the magnetic field direction. Indeed, it was possible to record either line (a) or (b) (Fig. 7) only by acting on the sample holder which could turn 0.3° at most in the cryostat. In order to study this anomaly, we have used sample 2 with its rotating sample holder. The result is reported in Fig. 8. The relative variation of the linewidth as a function of the magnetic field orientation does not exceed 20% about 1200 Oe and the splitting of the peak appears for two clearly distinct orientations. These properties are consistent neither with a spin effect nor with the appearance of two slightly different periods. Furthermore, the linewidth value is not consistent with that obtained at lower ultrasonic frequency. Presently, we have no satisfactory interpretation of these experimental results.

V. DISLOCATION EFFECT

We have already considered dislocations in Secs. II and IV to account for the linewidth of the GQO peaks. Furthermore, the amplitude-dependent ultrasonic attenuation in metals is generally connected with dislocations. Our experimental results, in particular the strong influence of temperature and ultrasonic amplitude on the GQO peak height, are explicable in terms of the magnetic field effect on the electron-dislocation interaction. The basic features of this effect have been already presented elsewhere.[28] The dislocations in the acoustical beam are treated as vibrating strings the motions of which are damped by the electrons. In the presence of a high magnetic field such that the Landau levels are well defined (i.e., $\hbar\Omega \gg kT$ and $\Omega\tau \gg 1$), the dislocation motions are damped as often as a Landau level reaches the Fermi level when the magnetic field is swept. The damping factor is of the form[28]

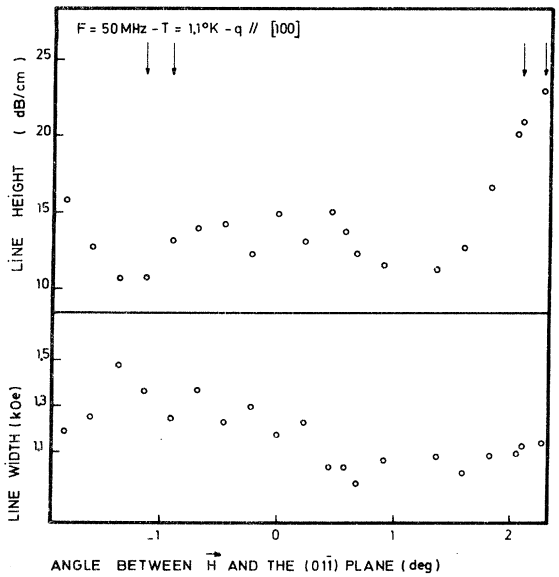

FIG. 8. Peak splitting as a function of the magnetic field direction with respect to the symmetry plane. The arrows show the magnetic field directions in which the peak is split.

$$B=\frac{C^2b^2m_c}{4\hbar}\sum_n\frac{\hbar\Omega}{4\pi^2}\left(\frac{2m_{\parallel}}{\hbar^2}\right)^{3/2}(E_F-n\hbar\Omega)^{-1/2}, \quad (25)$$

where $\vec{b}$ is the Burgers vector and C an interaction constant. It is found to be about 10^{-6} g cm^{-1} sec^{-1} when a Landau level is at the Fermi level. The dislocations are more free to move when $E_F \neq n\hbar\Omega$ than when $E_F = n\hbar\Omega$. Hence the ultrasonic-energy absorption by the dislocations is larger in the former case than in the latter (we consider here the amplitude-dependent type of loss[29]), and there are dips in the ultrasonic attenuation versus magnetic field.

The experimental attenuation dips are explained by the preceding mechanism. At 4.2 K the GQO peaks do not exist but the Landau levels are still well defined. Under the ultrasonic stress, the breaking away of the dislocations from the pinning impurities is realized as a result of the thermal agitation[30] which is large in mercury at 4.2 K. Thus, we are in the ultrasonic-amplitude range where the ultrasonic attenuation by the dislocations decreases when the ultrasonic amplitude increases.[29] Consequently, the dip height is smaller for the first echo than for the second one (Fig. 6). Taking into account these attenuation dips, we can then explain the GQO peak behavior. In the low-amplitude case and below 0.7 K (Fig. 5), the dislocations are pinned down by the impurities and the amplitude-dependent type of loss is absent. The peak is inhomogeneous, as we have seen in Sec. IV, and does not change with temperature. When T is increased above 0.7 K, because of thermal agitation the dislocations can break away from the pinning impurities and the amplitude-dependent type of loss can appear. When one sweeps the magnetic field, the resulting attenuation dips are added to the GQO peaks and make them disappear. In the high-amplitude case (Fig. 5), the dislocations are unpinned from the impurities throughout the temperature range 0.5–1.1 K. The attenuation dips are still present but have now a constant height. The inhomogeneous GQO peak does not change with temperature since $X = 6.5$ K and $T \leq 1.1$ K. Thus, for a fixed ultrasonic amplitude the resulting peak does not change in all the temperature range.

VI. CONCLUSIONS

The period measurements of the GQO corresponding to the β arms of the Fermi surface are in good agreement with those obtained by other means. On the other hand, the line-shape behavior cannot be explained using only the theory of Kaner and Skobov.[12] By taking into account the dislocation effect, most of the experimental results are interpreted. The dislocation damping by the electrons yields attenuation dips which add to the GQO peaks, and it is the resulting curve which is recorded. It is the same group of electrons which damps the dislocations and the ultrasonic wave. The typical values of the wave vector associated with the dislocation strain field are much larger than the usual values of the ultrasonic wave vector.[31,32] It suggests that the magnetic field effect on the dislocation damping always has to be considered at the same time as the Landau damping of the ultrasonic wave.

ACKNOWLEDGMENTS

The author is grateful to Professor R. G. Chambers and Professor J. Friedel for valuable discussions, and wishes to thank Professor W. Mercouroff, Dr. R. Reich, M. Ribault, and P. Demianozuk for their assistance. He is indebted to Dr. J. Grodski for a reading of the manuscript.

---

*Part of a Doctorat d'Etat thesis submitted at the University of Paris-Sud.

†Laboratoire associé au CNRS.

[1]V. L. Gurevitch, V. G. Skobov, and Yu. A. Firsov, Zh. Eksp. Teor. Fiz. **40**, 786 (1961) [Sov. Phys.-JETP **13**, 552 (1961)].

[2]A. P. Korolyuk and T. A. Prushchak, Zh. Eksp. Teor. Fiz. **41**, 1689 (1961) [Sov. Phys.-JETP **14**, 1201 (1962)].

[3]A. Myers and J. R. Bosnell, Phys. Lett. **17**, 9 (1965).

[4]L. R. Testardi and R. R. Soden, Phys. Rev. **158**, 581 (1967).

[5]A. P. Korolyuk, Fiz. Tverd. Tela **5**, 3323 (1963) [Sov. Phys.-Solid State **5**, 2433 (1964)].

[6]A. M. Toxen and S. Tansal, Phys. Rev. 137, A211 (1965).

[7]S. Mase, Y. Fujimori, and H. Mori, J. Phys. Soc. Jap. **21**, 1744 (1966).

[8]Y. Sawada, E. Burstein, and L. Testardi, J. Phys. Soc. Jap. Suppl. **21**, 760 (1966).

[9]Y. Shapira and B. Lax, Phys. Rev. 138, A1191 (1965).

[10]T. Fukase and T. Fukuroi, J. Phys. Soc. Jap. **23**, 650 (1967).

[11]G. Bellessa, M. Ribault, and R. Reich, Phys. Lett. A **31**, 556 (1970).

[12]E. A. Kaner and V. G. Skobov, Zh. Eksp. Teor. Fiz. 53, 375 (1967) [Sov. Phys.-JETP 26, 251 (1968)].

[13]E. V. Fenton and S. B. Woods, Phys. Rev. **151**, 424 (1966).

[14]R. B. Dingle, Proc. R. Soc. A **211**, 517 (1952).

[15]S. H. Liu and A. M. Toxen, Phys. Rev. 138, A487 (1965).

[16]The author is indebted to R. G. Chambers, who drew his attention to this broadening effect.

[17]R. G. Chambers, Proc. Phys. Soc. Lond. **89**, 695 (1966).

[18]A. H. Cottrell, S. C. Hunter, and F. R. N. Nabarro, Philos. Mag. **44**, 1064 (1953).

[19]A. Nourtier, J. Phys. (Paris) **33**, 135 (1972).

[20]The [100]* direction is the reciprocal-lattice vector which is normal to the (100) plane of the real lattice. Since the mercury structure is rhombohedral, the $[lmn]$ and $[lmn]^*$ directions are, in general, different.

[21]G. B. Brandt and J. A. Rayne, Phys. Rev. **148**, 644 (1966).

[22]S. C. Keeton and T. L. Loucks, Phys. Rev. **152**, 548 (1966).

[23]R. G. Poulsen, J. S. Moss, and W. R. Datars, Phys. Rev. B **3**, 3107 (1971).

[24]A. E. Dixon and W. R. Datars, Phys. Rev. **175**, 928 (1968).

[25]What we call low amplitude has no absolute meaning because we do not know what is lost in the transducer-sample junction. In

this particular case, there was 70-V peak-to-peak on a 4-mm-diam piezoelectric transducer.
[26]G. Bellessa, R. Reich, and W. Mercouroff, J. Phys. (Paris) **30**, 823 (1969).
[27]T. Kjeldaas and T. Holstein, Phys. Rev. Lett. **2**, 340 (1959).
[28]G. Bellessa, Phys. Rev. Lett. **28**, 668 (1972).
[29]A. V. Granato and K. Lücke, in *Physical Acoustics*, edited by W. P. Mason (Academic, New York, 1966), Vol. 4A, p. 225.
[30]J. Friedel, *Dislocations* (Pergammon, New York, 1967), p. 357.
[31]B. R. Tittmann and H. E. Bömmel, Phys. Rev. **151**, 178 (1966).
[32]V. Ya. Kravchenko, Fiz. Tverd. Tela **8**, 927 (1966) [Sov. Phys.-Solid State **8**, 740 (1966)].

PHYSICAL REVIEW B VOLUME 7, NUMBER 6 15 MARCH 1973

Multi-Ion Interactions and Structures in Simple Metals*

Walter A. Harrison
Applied Physics Department, Stanford University, Stanford, California 94305
(Received 10 October 1972)

The total energy of simple metals is calculated formally to all orders in the pseudopotential. The leading term (in the pseudopotential expansion) of the n-ion interaction is obtained from the nth-order terms and the asymptotic form for large separations is evaluated explicitly. The resulting n-ion interaction is proportional to $(E_F/k_F)(\lambda/k_F)^n[\cos k_F(l_1+l_2+\cdots+l_n)]/l_1l_2\cdots l_n(l_1+l_2+\cdots+l_n)$, where the l_i are consecutive segments of a straight-line path connecting the n ions and λ is of the order of a pseudopotential form factor divided by the Fermi energy. This is to be summed over all continuous paths connecting the n ions. The familiar two-body interaction proportional to $(\cos 2k_F r)/r^3$ is a special case. The three-body interaction is found to be strongest when the three ions form a straight line and are separated by nearest-neighbor distances. The assumption that the influence of d-state hybridization upon this interaction dominates the determination of structures leads to the correct distribution of cubic and hexagonal structures among the monovalent and divalent metals and to appropriate high and low axial ratios among the hexagonal structures.

I. INTRODUCTION

The essence of pseudopotential theory,[1] as applied to simple metals, is a treatment of the interaction between electrons and ions as a perturbation. It is assumed at the outset that the complete solution of the electron-ion problem, within a self-consistent-field approximation, would yield a good description of the metal. The only important approximation made in the solution of that one-electron problem is the perturbation expansion, ordinarily carried to second order. This approach gives us not only a mathematical basis for treating the entire range of metallic properties, but also a conceptual basis for thinking about these systems.

An important conceptual feature of the theory is that the second-order energy can be written as a two-body central-force interaction between atoms. This is plausible physically since the terms in second-order perturbation theory may be thought of as two consecutive scattering events by a single electron; they can therefore involve only two atoms. The inclusion of third-order perturbation theory will introduce explicit three-body interactions, etc. A second important feature of the second-order theory is the form of the two-body interaction. The asymptotic form for large distances is readily calculated and is proportional to $(\cos 2k_F r)/r^3$, exhibiting the familiar Friedel oscillations. Furthermore, this asymptotic form remains qualitatively correct even to distances as small as the interatomic distance in the metal, as seen in Fig. 1.

In the present study we will carry these calculations to higher order in the pseudopotential and obtain the asymptotic form of the leading term in the multi-ion interactions. It is important to be clear about what is being included and what is not being included in this analysis. We are *not* systematically including all higher-order terms in the calculation of the total energy. In particular, such a complete calculation would require the self-consistent recalculation of the pseudopotential itself in each order; the configuration of an ion's neighbors would affect the pseudopotential on that ion. We will neglect this effect and in all orders write the pseudopotential as the superposition of identical ionic pseudopotentials centered on the ion nuclei, and in any applications will use the individual pseudopotential calculated self-consistently to first order. Secondly, in each order we will focus upon the multi-ion interaction which first occurs in that order. Thus in third order we will obtain the three-ion interaction but will not compute the additional two-body interaction which arises in third